PHYSICAL REVIEW FLUIDS **7**, 093904 (2022)

Quantitative theory for spikes and bubbles in the Richtmyer-Meshkov instability at arbitrary density ratios

Qiang Zhang [1,2,*] and Wenxuan Guo [1]

[1] *Research Center for Mathematics, Beijing Normal University, Zhuhai 519087, China*

[2] *Guangdong Provincial Key Laboratory of Interdisciplinary Research and Application for Data Science, BNU-HKBU United International College, Zhuhai 519087, China*

(Received 29 April 2021; accepted 14 September 2022; published 27 September 2022)

To predict the growth rates of spikes and those of bubbles at a Richtmyer-Meshkov unstable interface between two fluids of arbitrary density ratios and over the entire nonlinear evolution stage is very important. So far most theories are applicable to bubbles only. There are no accurate theories available in the literature for spikes in systems with finite density ratios. In this paper, we present a theory that is applicable to both spikes and bubbles. Our theoretical predictions are in good agreement with numerical data for both spikes and bubbles over a wide range of density ratios and with various initial conditions. The theoretical predictions also agree well with experimental results.

DOI: 10.1103/PhysRevFluids.7.093904

I. INTRODUCTION

When a shock wave collides with a material interface between two immiscible fluids of different densities, the interface becomes unstable. Such an instability is known as the Richtmyer-Meshkov instability (RMI) [1,2]. It plays an essential role in understanding supernova explosions, inertial confinement fusion, etc. Due to its significance in both science and engineering applications, it has been intensively studied and is of great interest in the research field of interfacial fluid mixing. See Refs. [3–5] for comprehensive reviews.

When the shock hits the material interface, it leads to interfacial mixing between the two fluids. A fundamental question for RMI is how the mixing layer grows with time. The mixing layer is characterized by the penetration of heavy/light fluid into light/heavy fluid, known as spikes/bubbles. Figure 1 illustrates the evolution of spikes and bubbles. Since the size of the mixing layer is the vertical distance between the spike tip and the bubble tip, it is critical to develop theories for the growth rates of spikes and bubbles.

For systems with an infinite density ratio, the Layzer-type method has been extensively adapted. This method was initially introduced by Layzer [6] to study vacuum bubbles in the gravity-driven interfacial instability, known as Rayleigh-Taylor instability. It was extended by Hecht *et al.* to study vacuum bubbles in RMI [7]. This method was later applied to bubbles in cylindrical geometry by Mikaelian [8], and to spikes by Zhang [9].

For systems with arbitrary density ratios, Goncharov [10] and Sohn [11] applied Layzer's method to bubbles with finite density ratios. Abarzhi studied high-order harmonic modes in the bubble velocity potential [12]. Goncharov also extended the study to spikes [10]. A study of the asymptotic growth rates of spikes and bubbles and dominant scaling behavior among these fingers can be found in Ref. [13].

*Corresponding author: mazq@uic.edu.cn

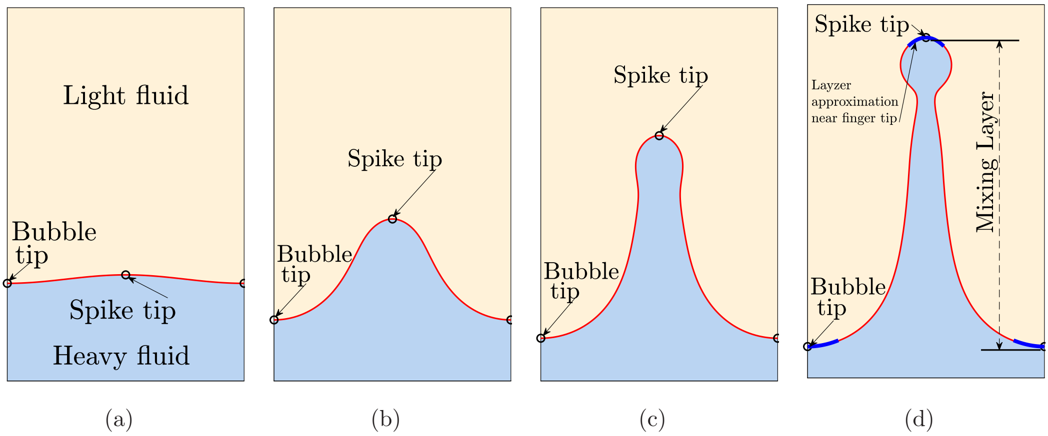

FIG. 1. Evolution of spikes and bubbles which characterize the development of the mixing layer in Richtmyer-Meshkov instability. The Layzer approximation approximates the shape of the interface near the tip of the finger as a parabola, shown as the blue curves in (d).

Spikes are more unstable than bubbles, and it is more difficult to predict the behavior of spikes. So far, there are no accurate theories for spikes in systems with arbitrary density ratios and over the whole nonlinear regime. The purpose of our study is to develop such a theory.

II. GOVERNING EQUATIONS

Richtmyer-Meshkov instability is generated by an incident shock. After hitting the material interface, the incident shock bifurcates into a transmitted shock and a reflected wave. The compressibility effects are important in the vicinity of these waves. However, as these waves propagate away from the material interface, the compressibility effects become less important and the nonlinear effects start to play a dominant role in the dynamics of spikes and bubbles. This transition occurs at the highest peak of compressible linear theory [see Fig. 5(b) of Ref. [14]]. Therefore, theoretical studies on the nonlinear behavior of spikes and bubbles in RMI consider incompressible, irrotational, and inviscid systems [7–13,15]. Following Refs. [7–13,15], we consider such a system in two dimensions governed by [6]

$$\nabla^2\phi_i(t,x,z) = 0, \tag{1}$$

$$\frac{\partial \eta}{\partial t} - \frac{\partial \phi_i}{\partial x}\frac{\partial \eta}{\partial x} + \frac{\partial \phi_i}{\partial z} = 0, \text{ at } z = \eta, \tag{2}$$

$$\sum_{i=1}^{2}(-1)^i\rho_i\left(\frac{\partial \phi_i}{\partial t} - \frac{1}{2}\left[\left(\frac{\partial \phi_i}{\partial x}\right)^2 + \left(\frac{\partial \phi_i}{\partial z}\right)^2\right]\right) = f(t), \text{ at } z = \eta. \tag{3}$$

Here, ϕ_i and ρ_i are the velocity potential and the density of fluid in phase i, respectively. Fluid 1 is on top of fluid 2. $z = \eta(t,x)$ denotes the location of the material interface at time t, and $f(t)$ is an arbitrary function that depends only on t. Following Layzer's approach [7–13,15], we approximate the shape of the interface near the finger tip (spike or bubble) by a parabola, namely, $\eta(t,x) = z_0(t) + \xi(t)kx^2$ [see the blue curves near the finger tips in Fig. 1(d)]. Here, k is the wave number of the initial perturbation, and $z_0(t)$ and $\xi(t)$ are the vertical location and curvature at the finger tip at time t, respectively. We define a signed Atwood number $A = (\rho_1 - \rho_2)/(\rho_1 + \rho_2)$. When $A > 0$ the finger is a bubble, and when $A < 0$ the finger is a spike. Following the approach in Ref. [13], ϕ_i is expressed in the following form:

$$\phi_i(t,x,z) = a_i(t)\cos(kx)e^{(-1)^i kz} + b_i(t)\cos[c(t)kx]e^{(-1)^i c(t)kz}, \quad i = 1,2. \tag{4}$$

Here, the term $\cos[c(t)kx]$ models the collective behavior of all modes beyond the primary mode $\cos(kx)$, and $c(t)$ depends on A [13]. After expanding Eqs. (1)–(4) through the order of x^2, one obtains a dynamic equation for the finger tip [13],

$$F_1\left[16\left(\frac{d\xi}{dt}\right)^2 - 10ckv\frac{d\xi}{dt} + c^2k^2v^2\right] + 2F_2\frac{d\xi}{dt}\frac{dc}{dt}$$
$$+ F_3kv\frac{dc}{dt} - F_4\left(2F_5\frac{d^2\xi}{dt^2} - F_6k\frac{dv}{dt}\right) = 0, \tag{5}$$

where $v = dz_0/dt$ is the finger growth rate. Here, F_1, F_2, F_3, F_4, F_5, and F_6 are functions of A, ξ, and c (see Ref. [13] for explicit expressions). Reference [13] shows that the asymptotic limits of $\xi(t)$, $c(t)$, and $v(t)$ are

$$\xi_\infty = \lim_{t\to\infty}\xi(t) = -\frac{3+A}{12\sqrt{2(1+A)}}, \tag{6}$$

$$c_\infty = \lim_{t\to\infty}c(t) = -6\xi_\infty, \tag{7}$$

and

$$\frac{dv}{dt} = -\alpha kv^2, \tag{8}$$

where

$$\alpha = \frac{3}{4}\frac{(1+A)(3+A)[4(3+A)+\sqrt{2}(9+A)(1+A)^{1/2}]}{[3+A+\sqrt{2}(1+A)^{1/2}][(3+A)^2+2\sqrt{2}(3-A)(1+A)^{1/2}]}. \tag{9}$$

The solution of Eq. (8) gives the asymptotic growth rate of fingers valid at large times,

$$v = \frac{v_0}{1+\alpha kv_0t}, \tag{10}$$

where $v_0 \equiv v(t=0)$ is the initial growth rate.

III. METHODOLOGY AND SOLUTIONS

We now include the preasymptotic behavior of these quantities. We perform an asymptotic expansion for $d\xi/dz_0$ in terms of $\xi - \xi_\infty$. Since $d\xi/dz_0 = 0$ at $\xi = \xi_\infty$, after expanding $d\xi/dz_0$ up to the second order in $\xi - \xi_\infty$, we have

$$\frac{d\xi}{dz_0} = -\frac{\beta k}{\xi_\infty + R}(\xi + R)(\xi - \xi_\infty), \tag{11}$$

where R is a constant and $\beta > 0$ is the decay rate. Both R and β depend on A and are to be determined. Similarly, we introduce the leading-order preasymptotic correction of c in terms of $\xi - \xi_\infty$, namely $c = c_\infty + S(\xi - \xi_\infty)$, where S is an A-dependent constant to be determined. This leads to the following solutions:

$$v = v_0e^{-\alpha k(z_0-a_0)}\left[\frac{\lambda_0+\lambda_1}{\lambda_0+\lambda_1e^{-\beta k(z_0-a_0)}}\right]^{1/(\beta\lambda_1)}, \tag{12}$$

$$\frac{dv}{dt} = -\left[\alpha - \frac{e^{-\beta k(z_0-a_0)}}{\lambda_0+\lambda_1e^{-\beta k(z_0-a_0)}}\right]kv^2. \tag{13}$$

Here, $a_0 \equiv z_0(t=0)$ is the initial amplitude of the perturbation, α is given by Eq. (9), and λ_0 and λ_1 are functions of R and S. The derivation for Eqs. (12) and (13) is given in Appendix A. Since solving R and S is equivalent to solving λ_0 and λ_1, we now determine λ_0 and λ_1. The small-time solution of the finger growth rate is [14]

$$v = v_0 - (A + a_0 k)kv_0^2 t + \left(A^2 - \frac{1}{2} + 2Aa_0 k\right)k^2 v_0^3 t^2 + O(t^3). \tag{14}$$

By matching the small-time behavior of Eq. (12) with Eq. (14), we obtain

$$\lambda_0 = \frac{1}{\beta(\alpha - A)^2}\left(1 + \frac{2a_0 k}{\alpha - A}\right), \tag{15}$$

$$\lambda_1 = \left[\frac{1}{\alpha - A} - \frac{1}{\beta(\alpha - A)^2}\right] + \left[\frac{1}{(\alpha - A)^2} - \frac{2}{\beta(\alpha - A)^3}\right]a_0 k. \tag{16}$$

The derivation for Eqs. (15) and (16) above is given in Appendix B.

Finally, we need to determine $\beta(A)$. It is shown in Ref. [13] that spikes and bubbles have a Laurent expansion in terms of $\sqrt{1+A}$. The three leading terms of $\beta(A)$ are

$$\beta(A) = \frac{h_{-1}}{\sqrt{1+A}} + h_0 + h_1\sqrt{1+A}. \tag{17}$$

To determine h_{-1}, h_0, and h_1, we examine the cases of infinite-density-ratio systems, namely, $A = 1$ and $A = -1$. Under the same Layzer approximation, the bubble and spike growth rates for an infinite-density-ratio system are given by $v = v_0[\frac{3(1\pm 2\xi_0)}{1\pm 6\xi_0 + 2e^{\pm 3k(z_0 - a_0)}}]^{1/2}$, where $\xi_0 \equiv \xi(t=0)$ is the initial curvature at the finger tip, "$\pm$" is taken as "$+$" for bubbles, and taken as "$-$" for spikes [9]. At large z_0, this result has the asymptotic expressions $v = v_0(\frac{3}{2})^{1/2}e^{-\frac{3}{2}k(z_0 - a_0)}[1 + O(a_0 k)]$ for bubbles ($A = 1$) and $v = v_0[\frac{3}{1+2e^{-3k(z_0-a_0)}}]^{1/2}[1 + O(a_0 k)]$ for spikes ($A = -1$). On the other hand, Eq. (12) has the asymptotic expressions $v = v_0(\frac{\beta}{2})^{\frac{1}{2\beta-4}}e^{-\frac{3}{2}k(z_0-a_0)}[1 + O(a_0 k)]$ for $A = 1$ and $v = v_0[\frac{\beta}{1+(\beta-1)e^{-\beta k(z_0-a_0)}}]^{\frac{1}{\beta-1}}[1 + O(a_0 k)]$ for $A = -1$. This leads to $\beta(1) = \beta(-1) = 3$. From these results and Eq. (17), we obtain $h_{-1} = h_1 = 0$ and $h_0 = 3$, namely $\beta(A) = 3$ for all A. After substituting $\beta(A) = 3$ into Eqs. (12), (15), and (16), we obtain the final analytic expression of the growth rate

$$v = v_0 e^{-\alpha k(z_0 - a_0)}\left[\frac{\lambda_0 + \lambda_1}{\lambda_0 + \lambda_1 e^{-3k(z_0 - a_0)}}\right]^{1/(3\lambda_1)}, \tag{18}$$

where

$$\lambda_0 = \frac{1}{3(\alpha - A)^2}\left(1 + \frac{2a_0 k}{\alpha - A}\right), \tag{19}$$

$$\lambda_1 = \left[\frac{1}{\alpha - A} - \frac{1}{3(\alpha - A)^2}\right] + \left[\frac{1}{(\alpha - A)^2} - \frac{2}{3(\alpha - A)^3}\right]a_0 k, \tag{20}$$

and α is given by Eq. (9). Since $\alpha - A \geqslant 1/2$ for $A \in [-1, 1]$, λ_0 and λ_1 given above are finite for all A. From $v = dz_0/dt$, the relation between t and z_0 can be solved from Eq. (18):

$$t = (kv_0)^{-1}\int_0^{k(z_0 - a_0)} e^{\alpha x'}\left[\frac{\lambda_0 + \lambda_1 e^{-3x'}}{\lambda_0 + \lambda_1}\right]^{1/(3\lambda_1)} dx'. \tag{21}$$

Equations (18) and (21) show that we express the growth rate v as a function of time t in a parametric form. We comment again, in Eqs. (18)–(21), $A < 0$ is for spikes and $A > 0$ is for bubbles. In particular, when $A = \pm 1$, Eq. (18) recovers the behavior of bubbles and that of spikes in an infinite-density-ratio system [9].

IV. VALIDATION STUDIES AND DISCUSSIONS

In Figs. 2 and 3, we compare our theoretical predictions given by Eqs. (18) and (21) (shown as blue solid curves) with numerical results (shown as black circles) from Ref. [16] and from Ref. [17], respectively. Both sets of numerical simulations are conducted in two dimensions. The numerical simulations in Fig. 2 are carried out with the FLASH code, an adaptive-mesh hydrodynamics code that solves Euler's equations for compressible inviscid flows [16]. In Fig. 2, the parameters are $A = \pm 0.98, \pm 0.94, \pm 0.88, \pm 0.75, \pm 0.5, \pm 0.25$, and $a_0 k = 0.125$. The numerical results in Fig. 3 are based on the point vortex method [17]. Applying the Biot-Savart law, the method converts a two-phase partial differential equation for incompressible inviscid flows into an array of point vortices on the material interface. In Fig. 3, the parameters are $A = \pm 1$, ± 0.7, ± 0.3, 0, and $a_0 k = 0.5$. In Figs. 2 and 3, the outset graphs are for spikes ($A \leqslant 0$) and the inset graphs are for bubbles ($A \geqslant 0$). The predictions given by Goncharov's theory [10] are also presented in Figs. 2 and 3 (shown as red dashed curves). The inset graphs show that both Goncharov's predictions and our predictions agree with the numerical results for bubbles quite well. This is due to the fact that the asymptotic bubble curvature is not sensitive to A: It only varies from $-\sqrt{2}/8 \approx -0.177$ for $A = 0$ to $-1/6 \approx -0.167$ for $A = 1$ [13]. Therefore, Goncharov's model which approximates the asymptotic curvature with $-1/6$ for all Atwood numbers is reasonable for bubbles. However, the situation is very different for spikes. For spikes, our predictions are still in good agreement with the numerical results. Figures 2 and 3 show that Goncharov's predictions for spikes deviate significantly from the numerical results at large density ratios. As commented by Mikaelian [18], "[Goncharov's] model overestimates simulations with small [initial amplitude] and underestimates for large [initial amplitude]." Figure 3(a) also shows that Goncharov's prediction for the spike growth rate is qualitatively incorrect. This is due to the fact that the asymptotic spike curvature is always $-1/6$ for all A in Goncharov's theory, but it should vary from $-\sqrt{2}/8 \approx -0.177$ for $A = 0$ to $-\infty$ for $A = -1$ [9,13].

Figures 2 and 3 show that the bubble growth rate always decreases with time. However, for spikes, the growth rate in certain cases [such as in Figs. 2(a)–2(d)] increases initially and then decreases. In other cases, it decreases monotonically with time, e.g., in Figs. 3(c) and 3(d). Now we provide an explanation for this behavior. From Eqs. (9), (13), (19), and (20), $\frac{dv}{dt}$ is negative for all $t > 0$ when $A \geqslant 0$. Therefore, the bubble growth rate always decreases monotonically with time. For spikes ($A < 0$), the growth rate will increase with time when $\alpha < \frac{e^{-3k(z_0 - a_0)}}{\lambda_0 + \lambda_1 e^{-3k(z_0 - a_0)}}$. This is only possible for spikes ($A < 0$) and $a_0 k < -A(1 - A/\alpha)$ (see Appendix C for the derivation of these criteria). Therefore, for a system with a large density ratio and a small perturbation amplitude, the spike growth rate will increase at early times and decrease at late times. Consequently, there is a maximum growth rate $v^* = v_0 (\frac{\alpha\lambda_0}{1-\alpha\lambda_1})^{\alpha/3} [\frac{(\lambda_0+\lambda_1)(1-\alpha\lambda_1)}{\lambda_0}]^{1/(3\lambda_1)}$ that occurs at $t^* = (3kv_0)^{-1} \int_{\alpha\lambda_0/(1-\alpha\lambda_1)}^{1} \zeta^{-\frac{\alpha}{3}-1} [\frac{\lambda_0+\lambda_1\zeta}{\lambda_0+\lambda_1}]^{1/(3\lambda_1)} d\zeta$. Namely, v increases in $[0, t^*]$ and decreases in $[t^*, \infty]$. The physical explanation for this phenomenon is as follows. There are two competing factors that determine the behavior of the finger growth rate. The first one is the effect of unstable growth generated by the incident shock. This effect tends to increase the growth rates for spikes and bubbles. The second effect is the energy constraint for each finger type. As a finger grows in magnitude, more and more fluid of one phase penetrates into the other. This increases the volume of the finger. The incident shock only deposits a certain amount of energy to the fluids. The increment of the finger volume requires a reduction of the growth rate to maintain overall energy conservation. For bubbles, the finger width increases with time. Therefore, it does not allow fast penetration due to energy constraint. Consequently, the energy constraint effect dominates the instability effect, and the bubble growth rate always decreases with time. For spikes, the finger width decreases with time. This allows deep penetration. When the initial amplitude is small, the volume of the spike is also small. As the spike becomes narrower, it penetrates deeper. Consequently, the instability effect dominates the energy constraint effect, and the spike growth rate increases at early times. Eventually, the volume of the spike becomes large. Then the energy constraint effect dominates, and the spike

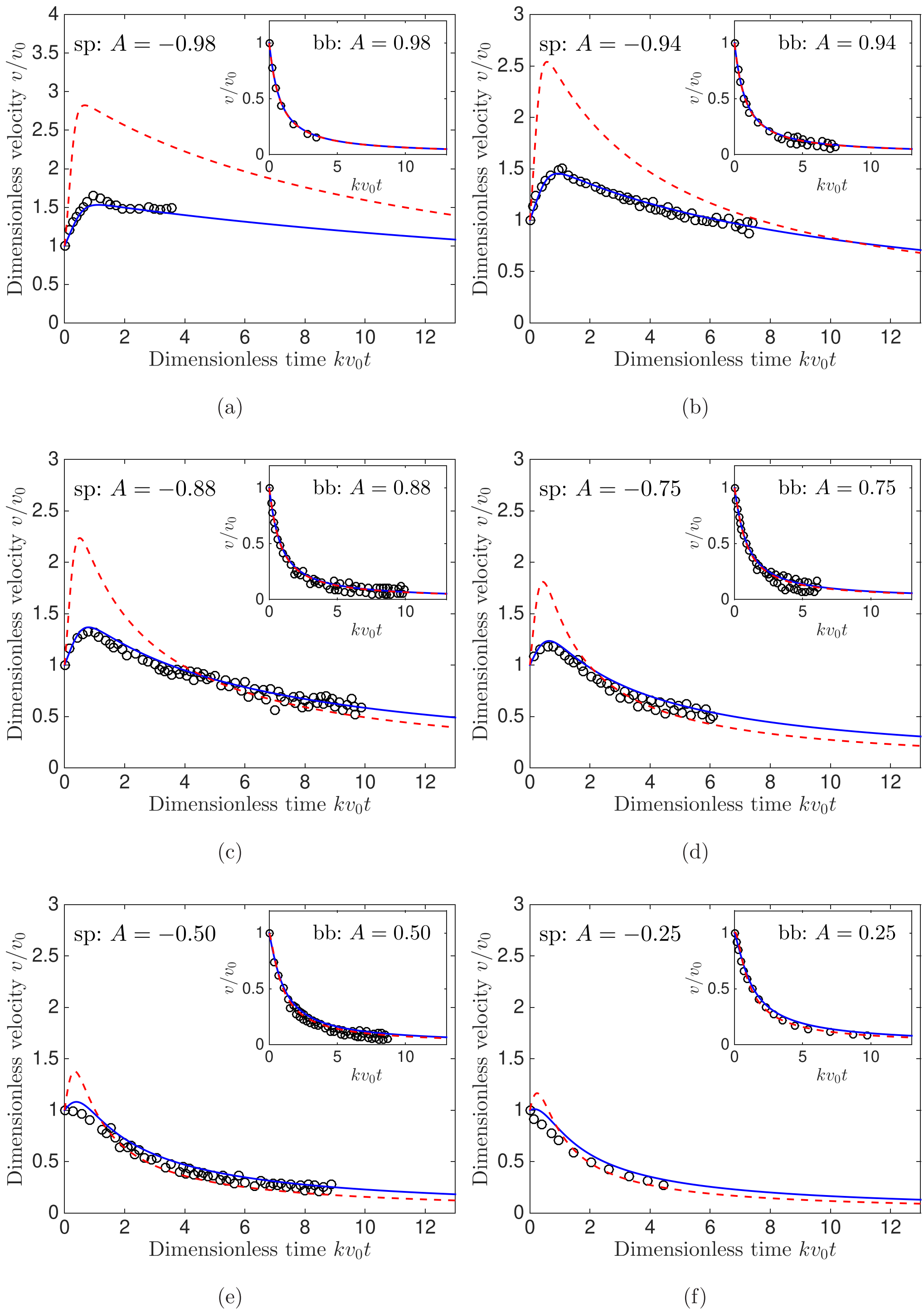

FIG. 2. Comparisons between theoretical predictions given by Eqs. (18) and (21) (blue solid curves), theoretical predictions given by Goncharov [10] (red dashed curves), and numerical results from Ref. [16] (black circle marks) for $a_0k = 0.125$ and various Atwood numbers $A = \pm0.98, \pm0.94, \pm0.88, \pm0.75, \pm0.5, \pm0.25$. Outsets: Growth rates for spikes. Insets: Growth rates for the corresponding bubbles.

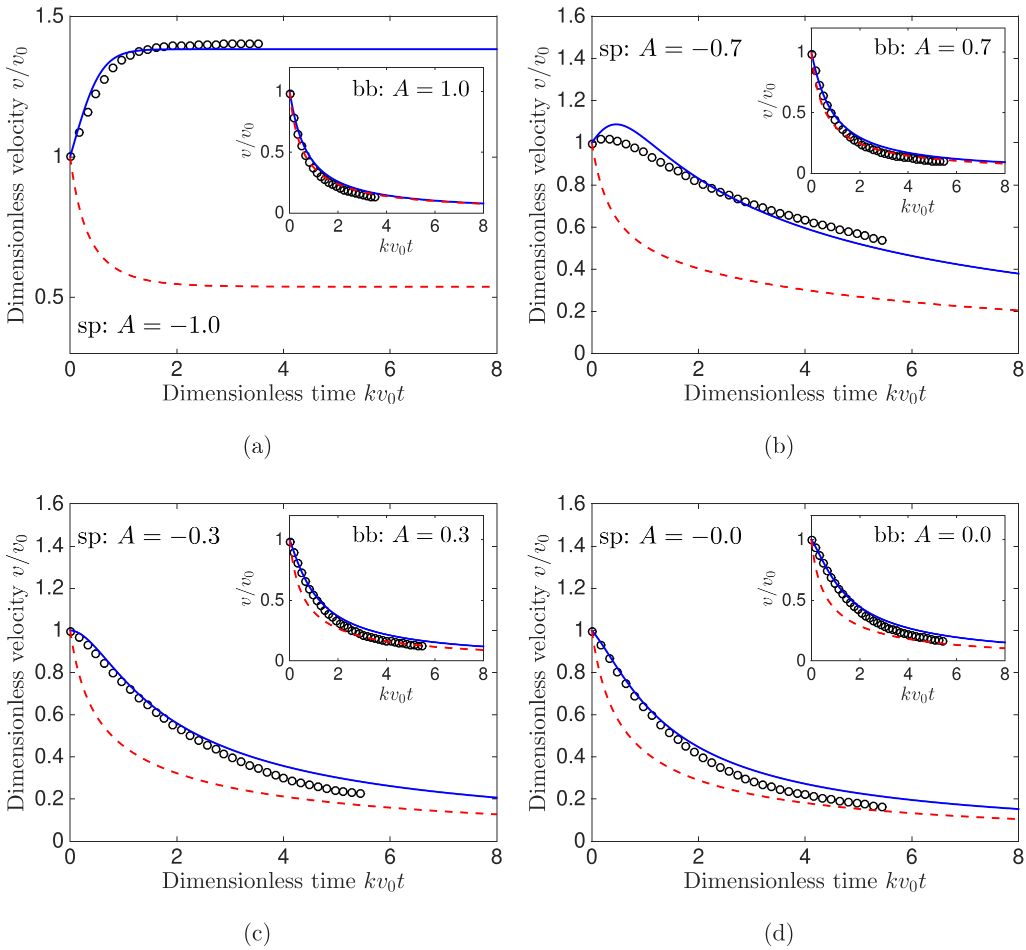

FIG. 3. Comparisons between theoretical predictions given by Eqs. (18) and (21) (blue solid curves), theoretical predictions given by Goncharov [10] (red dashed curves), and numerical results from Ref. [17] (black circle marks) for $a_0k = 0.5$ and various Atwood numbers $A = \pm 1, \pm 0.7, \pm 0.3, 0$. Outsets: Growth rates for spikes. Insets: Growth rates for the corresponding bubbles.

growth rate starts to decrease. The transition time t^* represents the transition point at which the energy constraint effect starts to dominate the instability effect. v^* is the largest growth rate that the spike can achieve. The larger the density ratio is, the narrower the spike becomes, and the larger v^* reaches. This is clearly shown in Fig. 2. For an infinite-density-ratio system, i.e., when $A = -1$, the spike curvature approaches infinity and the spike width approaches zero asymptotically. In this case, the spike grows with a constant velocity asymptotically, and the instability effect always dominates. For spikes ($A < 0$), when a_0k is larger than $-A(1 - A/\alpha)$, the initial volume of the spike is already large enough. In this case, the energy conservation effect dominates from the very beginning, and the spike growth rate decreases with time monotonically. The criterion for whether the instability effect dominates at early times can be easily determined at the initial time $t = t_0$, i.e., $z_0 = a_0$. From Eq. (13), the criterion is the sign of $q = \frac{1}{\lambda_0+\lambda_1} - \alpha$: When $q > 0$, the instability effect dominates initially; when $q < 0$, the energy conservation effect dominates all the time. For bubbles, q is always negative. For spikes, q is positive in Figs. 2(a)–2(f), 3(a), and 3(b), and q is negative in Figs. 3(c)

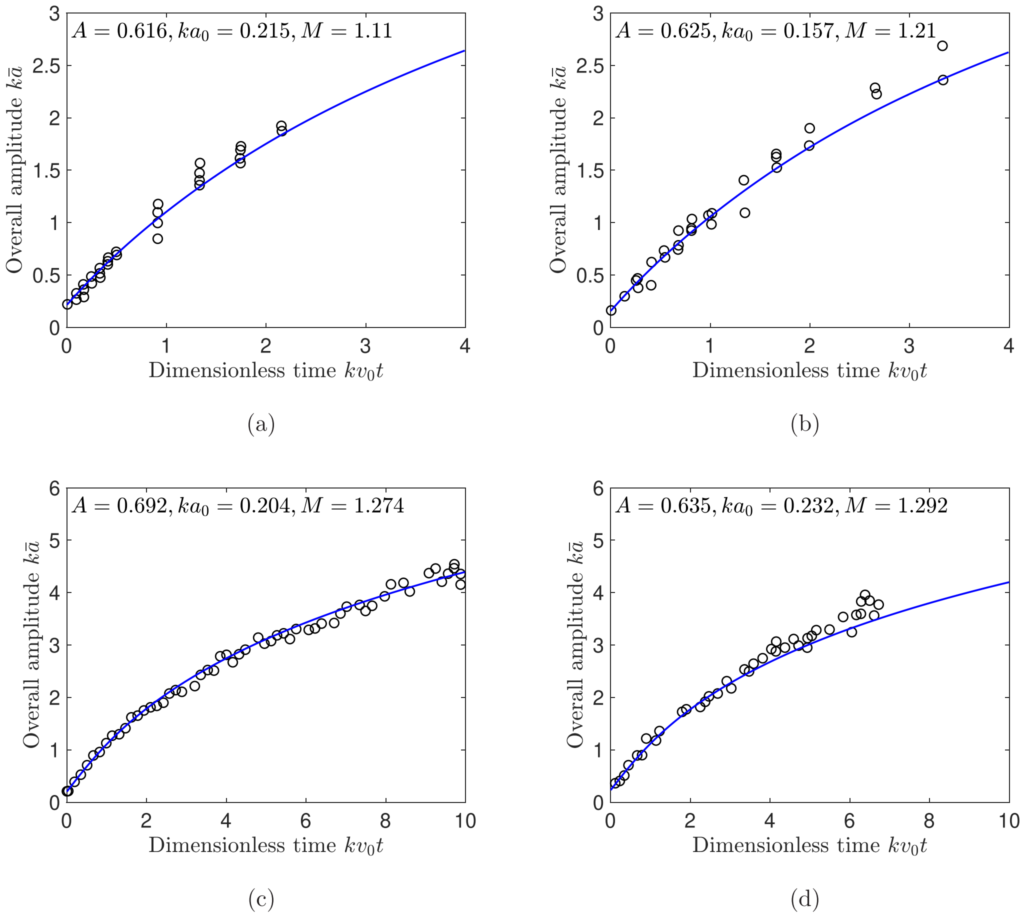

FIG. 4. Comparisons between theoretical predictions given by Eq. (21) (blue solid curves) and experimental data (black circle marks). The data in (a) and (b) are from Ref. [19]. The data in (c) and (d) are from Ref. [20]. The parameters are listed in the individual subpanels.

and 3(d). Note that for the spike in Fig. 2(f), q is a positive value but very close to zero, and t^* is small. This makes the small initial increment of the spike growth rate in Fig. 2(f) unobvious.

In Fig. 4, we compare our theoretical predictions with the experimental data from Refs. [19,20] for the overall amplitude, defined by a half of the vertical distance between the spike tip and the bubble tip, namely $\bar{a}(A, t) = [z_0(A, t) + z_0(-A, t)]/2$. Figure 4(a) is for $A = 0.616$, $ka_0 = 0.215$, $M = 1.11$ [19]. Here, A is the postshock Atwood number, a_0 is the postshock initial amplitude, and M is the Mach number of the incident shock. Figure 4(b) is for $A = 0.625$, $ka_0 = 0.157$, $M = 1.21$ [19]. Figure 4(c) is for $A = 0.692$, $ka_0 = 0.204$, $M = 1.274$ [20]. Figure 4(d) is for $A = 0.635$, $ka_0 = 0.232$, $M = 1.292$ [20]. Figure 4 shows that our theoretical predictions are also in good agreement with experimental data.

Our analytical solution given by Eqs. (18) and (21) is based on the method of asymptotic matching. It requires the information about the small-time solution given by Eq. (14) [14], the asymptotic large-time solution given by Eq. (10) [13], and the decay rate toward the asymptotic large-time solution, namely the parameter β derived in this paper. In Fig. 5, we compare the results from the small-time solution given by Eq. (14), from the asymptotic large-time solution given by Eq. (10), from our asymptotically matched solution given by Eqs. (18) and (21), and the data from

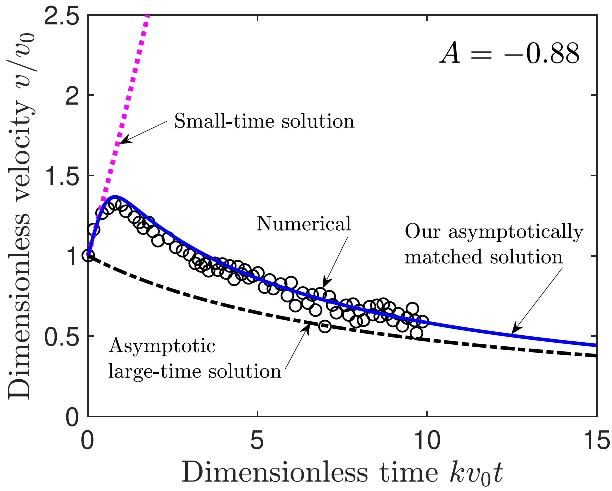

FIG. 5. Comparison for the spike growth rate between the results from the asymptotically matched solution given by Eqs. (18) and (21) (blue solid curve), from the asymptotic large-time solution in Ref. [13] (black dashed-dotted curve), from the small-time solution in Ref. [14] (magenta dotted curve), and the numerical results in Ref. [16] (black circle marks). The physical parameters are the same as in Fig. 2(c). The figure shows that the small-time solution, the asymptotic large-time solution, and the asymptotically matched solution presented in this paper agree with the numerical results at early times, at late times, and over the entire time domain, respectively.

numerical simulations. The physical parameters in Fig. 5 are the same as in Fig. 2(c). Figure 5 shows that the small-time solution, the asymptotic large-time solution, and the asymptotically matched solution agree with the numerical results at early times, at late times, and over the entire time domain, respectively. Particularly, the asymptotically matched solution given by Eqs. (18) and (21) recovers the small-time behavior given by Eq. (14) at early times, and approaches the large-time behavior given by Eq. (10) at late times. Since the asymptotic solution given by Eq. (10) is for the large-time behavior only, it contains no effect of initial unstable growth in the spike development but the energy constraint effect discussed earlier. Therefore, the asymptotic large-time solution decreases monotonically with time and is smaller than the asymptotically matched solution and the numerical data.

V. SUMMARY

In summary, we present an analytical solution for the growth rate of spikes and bubbles in Richtmyer-Meshkov instability. This solution is for arbitrary density ratios and for the entire nonlinear evolution process over all times. The theoretical predictions are in good agreement with numerical results and with experimental data over a large range of density ratios.

ACKNOWLEDGMENTS

The work of Q.Z. was supported in part by The National Natural Science Foundation of China (Grant No. 12272054); in part by the Research Grants Council of the HKSAR, China (Project No. CityU 11302919); in part by Guangdong Provincial Key Laboratory of Interdisciplinary Research and Application for Data Science, BNU-HKBU United International College (Project No. 2022B1212010006); and in part by Guangdong Higher Education Upgrading Plan (2021-2025) (Project No. UIC R0400024-21).

APPENDIX A: DERIVATION DETAIL FOR EQS. (8) AND (9) IN THE MAIN TEXT

In this Appendix, we provide the derivation details for Eqs. (12) and (13) in the main text. Equation 11 in the main text is the asymptotic expansion for $d\xi/dz_0$ in terms of $\xi - \xi_\infty$, namely

$$\frac{d\xi}{dz_0} = -\frac{\beta k}{\xi_\infty + R}(\xi + R)(\xi - \xi_\infty), \tag{A1}$$

where R and β are constants to be determined. From this equation, we have

$$\frac{d^2\xi}{dz_0^2} = -\frac{\beta k}{\xi_\infty + R}(2\xi - \xi_\infty + R)\frac{d\xi}{dz_0} = \frac{\beta^2 k^2}{(\xi_\infty + R)^2}(2\xi - \xi_\infty + R)(\xi + R)(\xi - \xi_\infty). \tag{A2}$$

Similarly, we also apply a preasymptotic correction of c in terms of $\xi - \xi_\infty$:

$$c = c_\infty + S(\xi - \xi_\infty), \tag{A3}$$

where S is a constant to be determined. From Eq. (A3), we have

$$\frac{dc}{dz_0} = S\frac{d\xi}{dz_0} = -\frac{\beta S k}{\xi_\infty + R}(\xi + R)(\xi - \xi_\infty). \tag{A4}$$

Since

$$\frac{d\xi}{dt} = v\frac{d\xi}{dz_0}, \quad \frac{d^2\xi}{dt^2} = v^2\frac{d^2\xi}{dz_0^2} + \frac{d\xi}{dz_0}\frac{dv}{dt}, \quad \text{and} \quad \frac{dc}{dt} = v\frac{dc}{dz_0}, \tag{A5}$$

based on Eqs. (A1)–(A5), Eq. (5) in the main text can be written as

$$\frac{dv}{dt} = -\frac{P(\xi)}{Q(\xi)}kv^2, \tag{A6}$$

with

$$P(\xi) = F_1\left[\frac{16}{k^2}\left(\frac{d\xi}{dz_0}\right)^2 - \frac{10c}{k}\frac{d\xi}{dz_0} + c^2\right] + \frac{2F_2}{k^2}\frac{d\xi}{dz_0}\frac{dc}{dz_0} + \frac{F_3}{k}\frac{dc}{dz_0} - \frac{2F_4F_5}{k^2}\frac{d^2\xi}{dz_0^2}, \tag{A7}$$

$$Q(\xi) = F_4\left(F_6 - \frac{2F_5}{k}\frac{d\xi}{dz_0}\right). \tag{A8}$$

Since $F_1, F_2, \ldots, F_6$ are functions of ξ and c, from Eqs. (A1)–(A5), both P and Q are functions of ξ only. To determine a preasymptotic solution with the leading-order correction, we only need to expand $P(\xi)$ and $Q(\xi)$ up to $O(\xi - \xi_\infty)$, namely,

$$P(\xi) = P(\xi_\infty) + P'(\xi_\infty)(\xi - \xi_\infty), \tag{A9}$$

$$Q(\xi) = Q(\xi_\infty) + Q'(\xi_\infty)(\xi - \xi_\infty). \tag{A10}$$

The expressions for $P(\xi_\infty)$, $P'(\xi_\infty)$, $Q(\xi_\infty)$, and $Q'(\xi_\infty)$, which are functions of R, S, and β, can be explicitly determined from the expressions of $F_1, F_2, \ldots, F_6$ and Eqs. (A1)–(A8), and will not be displayed here due to their lengthy expressions. In particular, one can check that

$$P(\xi_\infty)/Q(\xi_\infty) = \alpha(A), \tag{A11}$$

with $\alpha(A)$ given by Eq. (9) in the main text. Therefore, Eq. (A6) can be expressed as

$$\frac{dv}{dt} = -\frac{P(\xi_\infty) + P'(\xi_\infty)(\xi - \xi_\infty)}{Q(\xi_\infty) + Q'(\xi_\infty)(\xi - \xi_\infty)}kv^2 = -\left[\alpha + \frac{[P'(\xi_\infty) - \alpha\, Q'(\xi_\infty)](\xi - \xi_\infty)}{Q(\xi_\infty) + Q'(\xi_\infty)(\xi - \xi_\infty)}\right]kv^2. \tag{A12}$$

An analytical expression for ξ can be obtained from Eq. (A1),

$$\xi = \xi_\infty + \frac{e^{-\beta k(z_0 - a_0)}}{d_0 + d_1 e^{-\beta k(z_0 - a_0)}}, \tag{A13}$$

where

$$d_0 = \frac{\xi_0 + R}{(\xi_\infty + R)(\xi_0 - \xi_\infty)}, \quad d_1 = -\frac{1}{\xi_\infty + R}, \tag{A14}$$

and $a_0 \equiv z_0(t = 0)$ is the initial amplitude of the perturbation. After substituting Eq. (A13) into Eq. (A12), we have

$$\frac{dv}{dt} = -\left[\alpha - \frac{e^{-\beta k(z_0 - a_0)}}{\lambda_0 + \lambda_1 e^{-\beta k(z_0 - a_0)}}\right] k v^2, \tag{A15}$$

where

$$\lambda_0 = -\frac{d_0 Q(\xi_\infty)}{P'(\xi_\infty) - \alpha Q'(\xi_\infty)}, \quad \lambda_1 = -\frac{d_1 Q(\xi_\infty) + Q'(\xi_\infty)}{P'(\xi_\infty) - \alpha Q'(\xi_\infty)}. \tag{A16}$$

After substituting $\frac{dv}{dt} = \frac{dv}{dz_0}\frac{dz_0}{dt} = v\frac{dv}{dz_0}$ into Eq. (A15) and integrating the resulting equation over z_0, we obtain an explicit expression for the growth rate,

$$v = v_0 e^{-\alpha k(z_0 - a_0)} \left[\frac{\lambda_0 + \lambda_1}{\lambda_0 + \lambda_1 e^{-\beta k(z_0 - a_0)}}\right]^{1/(\beta\lambda_1)}, \tag{A17}$$

where $v_0 \equiv v(t = 0)$ is the initial growth rate. Equations (A17) and (A15) above are Eqs. (12) and (13) in the main text, respectively.

APPENDIX B: DETERMINATION DETAIL FOR λ_0 and λ_1

In this Appendix, by using the asymptotic matching method, we determine λ_0 and λ_1 displayed in Eqs. (15) and (16) of the main text. At $t = 0$, the solution of the growth rate, up to $O(a_0 k)$, has the following properties [see Eq. (14) in the main text]:

$$\left.\frac{dv}{dt}\right|_{t=0} = -(A + a_0 k) k v_0^2, \tag{B1}$$

$$\left.\frac{d^2 v}{dt^2}\right|_{t=0} = 2\left(A^2 - \frac{1}{2} + 2A a_0 k\right) k^2 v_0^3. \tag{B2}$$

The derivation of Eqs. (B1) and (B2) can be found in Ref. [14]. From Eq. (13), we have

$$\left.\frac{dv}{dt}\right|_{t=0} = -\left(\alpha - \frac{1}{\lambda_0 + \lambda_1}\right) k v_0^2, \tag{B3}$$

$$\begin{aligned}\left.\frac{d^2 v}{dt^2}\right|_{t=0} &= -2\left(\alpha - \frac{1}{\lambda_0 + \lambda_1}\right) k v_0 \left.\frac{dv}{dt}\right|_{t=0} - k v_0^3 \left[\frac{d}{dz_0}\left(\alpha - \frac{e^{-\beta k(z_0 - a_0)}}{\lambda_0 + \lambda_1 e^{-\beta k(z_0 - a_0)}}\right)\right]_{z=a_0} \\ &= 2\left(\alpha - \frac{1}{\lambda_0 + \lambda_1}\right)^2 k^2 v_0^3 - \frac{\beta\lambda_0}{(\lambda_0 + \lambda_1)^2} k^2 v_0^3. \end{aligned} \tag{B4}$$

By matching Eq. (B1) with Eq. (B3) and matching Eq. (B2) with Eq. (B4), one can solve λ_0 and λ_1 up to $O(a_0 k)$. The solutions are

$$\lambda_0 = \frac{1}{\beta(\alpha - A)^2}\left(1 + \frac{2a_0 k}{\alpha - A}\right), \tag{B5}$$

$$\lambda_1 = \left[\frac{1}{\alpha - A} - \frac{1}{\beta(\alpha - A)^2}\right] + \left[\frac{1}{(\alpha - A)^2} - \frac{2}{\beta(\alpha - A)^3}\right] a_0 k. \tag{B6}$$

Equations (B5) and (B6) above are Eqs. (15) and (16) in the main text, respectively.

APPENDIX C: DERIVATION OF THE CRITERIA FOR EARLY-TIME ACCELERATION

In this Appendix, we determine in which situation the finger will experience an acceleration at early times. From Eq. (13), the condition that the finger is in acceleration is

$$\frac{dv}{dt} = -\left[\alpha - \frac{e^{-3k(z_0-a_0)}}{\lambda_0 + \lambda_1 e^{-3k(z_0-a_0)}}\right] k v^2 > 0. \tag{C1}$$

Since $kv^2 > 0$, Eq. (C1) is equivalent to

$$\frac{\zeta}{\lambda_0 + \lambda_1 \zeta} > \alpha, \tag{C2}$$

where $\zeta = e^{-3k(z_0-a_0)}$. Note that for $z_0 \geqslant a_0$ we have $0 < \zeta \leqslant 1$. In this case, one can check that $\lambda_0 + \lambda_1 \zeta > 0$. Therefore, Eq. (C2) gives

$$(1 - \alpha\lambda_1)\zeta > \alpha\lambda_0. \tag{C3}$$

Since $\alpha \geqslant 0$, $\lambda_0 > 0$, and $\zeta > 0$, Eq. (C3) will only be satisfied when

$$1 - \alpha\lambda_1 > 0. \tag{C4}$$

This leads to

$$\zeta > \frac{\alpha\lambda_0}{1 - \alpha\lambda_1}. \tag{C5}$$

Consequently, if

$$\frac{\alpha\lambda_0}{1 - \alpha\lambda_1} < 1, \tag{C6}$$

there exists an interval $\frac{\alpha\lambda_0}{1-\alpha\lambda_1} < \zeta \leqslant 1$ in which $\frac{dv}{dt} > 0$. Substituting Eqs. (19) and (20) into Eq. (C6), we obtain the condition

$$a_0 k < -A\left(1 - \frac{A}{\alpha}\right). \tag{C7}$$

One can check that $1 - \frac{A}{\alpha} > 0$. Therefore, Eq. (C7) will be satisfied only when $A < 0$. Now we need to check whether Eq. (C4) is satisfied. After substituting Eq. (20) into Eq. (C4) and simplifying the resulting inequality, we obtain

$$a_0 k\left(-3 + \frac{2}{\alpha - A}\right) < 1 - 3(\alpha - A)\frac{A}{\alpha}. \tag{C8}$$

When $A < 0$, the right-hand side of Eq. (C8) is positive. Additionally, $\alpha - A > 2/3$ when $A < 0$. Hence, the left-hand side of Eq. (C8) is negative. Therefore, Eq. (C8) and equivalently Eq. (C4) are always satisfied when $A < 0$. This leads to the conclusion that when $A < 0$ and $a_0 k < -A(1 - \frac{A}{\alpha})$, the finger will experience an acceleration at early times. This is stated in the main text.

[1] R. D. Richtmyer, Taylor instability in shock acceleration of compressible fluids, Commun. Pure Appl. Math. **13**, 297 (1960).

[2] E. E. Meshkov, Instability of the interface of two gases accelerated by a shock wave, Fluid Dyn. **4**, 101 (1969).

[3] M. Brouillette, The Richtmyer-Meshkov instability, Annu. Rev. Fluid Mech. **34**, 445 (2002).

[4] Y. Zhou, Rayleigh–Taylor and Richtmyer–Meshkov instability induced flow, turbulence, and mixing. I, Phys. Rep. **720-722**, 1 (2017).

[5] Y. Zhou, Rayleigh–Taylor and Richtmyer–Meshkov instability induced flow, turbulence, and mixing. II, Phys. Rep. **723-725**, 1 (2017).

[6] D. Layzer, On the instability of superposed fluids in a gravitational field, Astrophys. J. **122**, 1 (1955).

[7] J. Hecht, U. Alon, and D. Shvarts, Potential flow models of Rayleigh-Taylor and Richtmyer-Meshkov bubble fronts, Phys. Fluids **6**, 4019 (1994).

[8] K. O. Mikaelian, Analytic Approach to Nonlinear Rayleigh-Taylor and Richtmyer-Meshkov Instabilities, Phys. Rev. Lett. **80**, 508 (1998).

[9] Q. Zhang, Analytical Solutions of Layzer-Type Approach to Unstable Interfacial Fluid Mixing, Phys. Rev. Lett. **81**, 3391 (1998).

[10] V. N. Goncharov, Analytical Model of Nonlinear, Single-Mode, Classical Rayleigh-Taylor Instability at Arbitrary Atwood Numbers, Phys. Rev. Lett. **88**, 134502 (2002).

[11] S.-I. Sohn, Simple potential-flow model of Rayleigh-Taylor and Richtmyer-Meshkov instabilities for all density ratios, Phys. Rev. E **67**, 026301 (2003).

[12] S. I. Abarzhi, Nonlinear evolution of unstable fluid interface, Phys. Rev. E **66**, 036301 (2002).

[13] Q. Zhang and W. Guo, Universality of finger growth in two-dimensional Rayleigh–Taylor and Richtmyer–Meshkov instabilities with all density ratios, J. Fluid Mech. **786**, 47 (2016).

[14] Q. Zhang and S.-I. Sohn, Nonlinear theory of unstable fluid mixing driven by shock wave, Phys. Fluids **9**, 1106 (1997).

[15] K. O. Mikaelian, Explicit expressions for the evolution of single-mode Rayleigh-Taylor and Richtmyer-Meshkov instabilities at arbitrary Atwood numbers, Phys. Rev. E **67**, 026319 (2003).

[16] G. Dimonte and P. Ramaprabhu, Simulations and model of the nonlinear Richtmyer-Meshkov instability, Phys. Fluids **22**, 014104 (2010).

[17] S.-I. Sohn, Vortex model and simulations for Rayleigh-Taylor and Richtmyer-Meshkov instabilities, Phys. Rev. E **69**, 036703 (2004).

[18] K. O. Mikaelian, Limitations and failures of the Layzer model for hydrodynamic instabilities, Phys. Rev. E **78**, 015303(R) (2008).

[19] B. D. Collins and J. W. Jacobs, PLIF flow visualization and measurements of the Richtmyer–Meshkov instability of an air/SF_6 interface, J. Fluid Mech. **464**, 113 (2002).

[20] J. W. Jacobs and V. V. Krivets, Experiments on the late-time development of single-mode Richtmyer–Meshkov instability, Phys. Fluids **17**, 034105 (2005).